Scattering of conduction electrons from vacancies in gold

B. Lengeler
Institut für Festkörperforschung, Kernforschungsanlage Jülich, D-5170 Jülich, Germany
(Received 21 January 1977)

Dingle temperatures for the scattering of conduction electrons at vacancies quenched into gold have been measured for 10 cyclotron orbits. The effect of dislocations produced during the quench has been separated from the contribution of the vacancies. Local values of the scattering rates are calculated from the data. The anisotropy of the scattering turns out to be very small. Vacancies in Au are characterized by a strong relaxation of the surrounding lattice. Calculations of Dingle temperatures for a vacancy model without lattice relaxation give a neck Dingle temperature which is only 50% of those for the belly orbits, whereas the measured value is smaller only by 10%. This discrepancy is due to the lattice distortion which increases preferentially the neck scattering and is therefore responsible for the weak anisotropy of the measured data. The scattering theories available at present time are not applicable to vacancies in Au. They must be extended to include the lattice distortion.

I. INTRODUCTION

The de Haas–van Alphen (dHvA) effect has been used extensively in the last years to investigate the scattering of conduction electrons from impurity atoms in dilute alloys. Most effort has been towards noble-metal alloys with substitutional[1-4] and interstitial[5] impurities. Among the structural defects studied by dHvA effect are edge dislocations[6] and dislocation loops produced by neutron irradiation[7] in Cu. In this paper a detailed analysis of scattering of conduction electrons from vacancies in Au will be presented. A new technique has been applied to quench-in the lattice vacancies present in thermal equilibrium at high temperatures.[8] Mainly single vacancies distributed randomly in the sample are quenched-in by this procedure. In addition, some 8×10^6 dislocations/cm^2 are created by the quick cooling of the samples. Dingle temperatures were measured for ten orbits in 11 samples containing up to 274 ppm of vacancies.

The paper is organized as follows. Section II describes briefly how the dHvA effect is used to determine scattering rates of the conduction electrons. The preparation of the samples with controlled vacancy concentrations is described in some length. The experimental results are given in Sec. III. It is described how the contributions of vacancies and dislocations to the scattering rates are separated. In Sec. IV local values of the scattering rates are deduced from the experimental data. A vacancy in Au is characterized by an especially strong distortion of the lattice around it. It is shown that any reasonable analysis of the data has to take into account this strong relaxation. The importance of the lattice relaxation is obvious from the calculation of Dingle temperatures using a simple model for a vacancy in Au.

II. EXPERIMENTAL

A. dHvA amplitude measurements

In a previous paper[5] we have described in some detail how the dHvA effect is used to determine the $\vec{k}$ dependence of the scattering rates $1/\tau^*(\vec{k})$ of conduction electrons from defects. Under suitable conditions the oscillatory magnetization varies in the following way with the temperature T and the magnetic field H,

$$M = M_0 \frac{T}{\sqrt{H}} \frac{\exp(-b\,m_c^* X^*/m_0 H)}{\sinh(b\,m_c^* T/m_0 H)} \sin\left(\frac{2\pi F}{H} + \gamma\right). \quad (1)$$

The constant b has the value 146.925 kG/K. M_0 and γ are independent of T and H. The magnetization varies sinusoidally in $1/H$ with the dHvA frequency F. The Landau-level broadening described by the Dingle temperature X^* and caused by the scattering of the conduction electrons from defects produces an exponential damping of the dHvA amplitudes. The Dingle temperature X^* given by

$$X^* = (\hbar/2\pi k_B)\ \langle 1/\tau^*(\vec{k})\rangle \quad (2)$$

is an orbital average $\langle\cdots\rangle$ of the local scattering rates $1/\tau^*(\vec{k})$ of the electrons around an extremal cross section. From measurements of the dHvA amplitudes $A(T,H)$ as a function of field H at fixed temperature T and a plot $\ln[A\sqrt{H}\sinh(b\,m_c^* T/m_0 H)]$ vs H^{-1} one obtains the Dingle temperature X^*. The cyclotron masses m_c^* used in the analysis were taken from Ref. 9. The Dingle temperatures and the cyclotron masses determined by dHvA effect are renormalized by electron-phonon interaction, and so are the local scattering rates $1/\tau^*(\vec{k})$.[5,9] This is the meaning of the asterisk on X^*, m_c^*, and τ^* in Eqs. (1) and (2).

The dHvA measurements were made by a field modulation technique. Details of the apparatus

and of the temperature, field, and amplitude measurements are given in Refs. 5 and 9.

B. Preparation of dHvA samples with controlled vacancy concentrations

The samples used in the experiment were cylindrical gold single crystals 1 mm in diameter and 5 mm in length with the axis of the cylinder in the ⟨110⟩ crystallographic direction. The samples were grown directly as cylinders 1 mm in diam by the Czochralski technique and cut to length by an electrolytic layer saw.[10] No spark erosion was applied. The samples were annealed for 3 h in air at 970 °C. The crystals had dislocation densities as low as 2000/cm^2 and a residual resistivity of 0.4 nΩ cm. Typical Dingle temperatures of the pure samples were 0.03 K for all orbits.

A new technique has been developed for quenching these high quality and delicate single crystals.[8] With this technique it has been possible for the first time to quench into a single crystal all the vacancies present at high temperatures in thermal equilibrium. Vacancy losses during the quenching procedure could be kept negligibly small. The quenching bath used was a mixture of water and hydrochloric acid cooled to −70 °C. It is necessary to keep the bath temperature appreciably below 0 °C since clustering of vacancies already starts at −20 °C. This has been shown by positron annihilation measurements on Au quenched from 950 °C with our technique and subsequently annealed isochronally.[11] The beginning of the vacancy clustering is hardly visible in the recovery of the residual electrical resistivity produced by the quenched-in vacancies. Figure 1 is an isochronal annealing curve for quenched Au. After quenching the sample is annealed for 30 min at the temperatures indicated by the circles in Fig. 1 and after each annealing period the residual resistivity $\Delta\rho$ is measured at 4.2 K. The large recovery stage centered at 50 °C is correlated with the clustering of vacancies in stacking-fault tetrahedra.[12] In view of the high quality of the crystals used and in view of the high quenching rate (3×10^4 °C/sec) and of the low bath temperature, it can be assumed that the quenched-in vacancies were mainly single vacancies. To avoid any clustering of the vacancies during the handling following the quench the samples were built into the sample holder and into the cryostat under liquid nitrogen at 77 K. The residual resistivity of vacancies in Au was found to be $\rho_v = (1.69 \pm 0.20)\ \mu\Omega$ cm/at.%.[8] The vacancy concentration in the samples investigated was determined from residual resistivity measurements using the above-quoted conversion factor ρ_v.

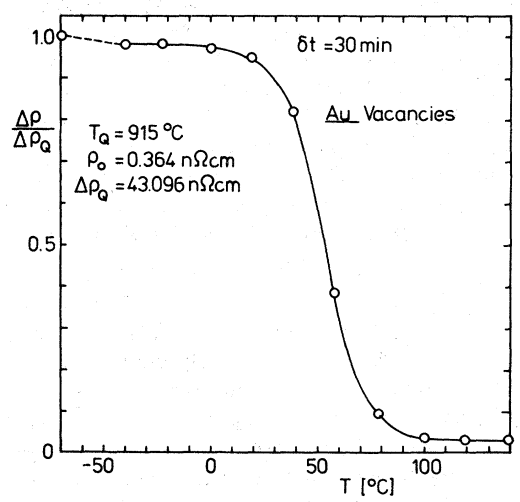

FIG. 1. Isochronal annealing of the residual electrical resistivity of a Au single crystal quenched from 915 to −70 °C. After quenching the crystal contained 255 ppm of vacancies. Big recovery stage centered at 50 °C is due to the clustering of vacancies in stacking-fault tetrahedra.

III. RESULTS

Dingle temperatures have been measured in 11 different Au single crystals for ten extremal cross sections in the plane {110}. The vacancy concentrations ranged from 0 to 274 ppm. Figure 2 shows some typical Dingle plots for a Au sample containing 255 ppm of vacancies. Great care was paid to the amplitude measurements. Systematic errors due to magnetic interaction and to incomplete penetration of the modulation field (30 Hz) into the sample were eliminated. B, N, D, and R stand for belly, neck, dogsbone, and four-cornered rosette. Numbers without brackets behind the orbit symbol give the angle by which the magnetic field is tilted against the crystallographic direction [001] in the plane {110}.

Figure 3 shows the Dingle temperatures X^* as a function of the vacancy concentration for four typical orbits. In addition to the contribution of X^* linear in the vacancy concentration there is a strong background scattering manifesting itself in an intercept at $c_v = 0$. The data points at $c_v \approx 0$ have been obtained from a sample quenched from 505 °C. At that temperature the concentration of vacancies in thermal equilibrium is as small as 1.7 ppm.[8] This sample showed only very little increase of the residual resistivity after quenching. We attribute the intercept at $c_v = 0$ to the scattering of conduction electrons at dislocations produced by the quench.

It is well known that the differential thermal contraction during the rapid cooling of a crystal creates lattice strain.[13] The exact amount of disloca-

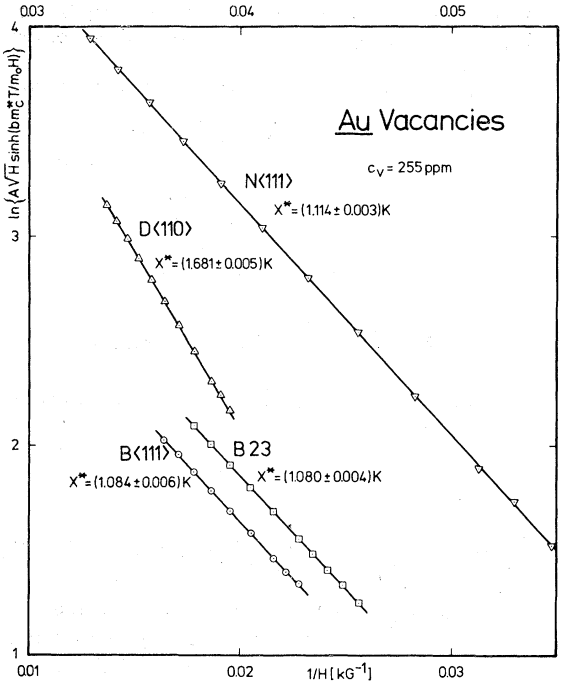

FIG.2. Dingle plots for four extremal cross sections in Au containing 255 ppm of vacancies. Lower abscissa holds for the B 23, $B\langle 111\rangle$, and $D\langle 110\rangle$ orbits, the upper for the $N\langle 111\rangle$ orbit. Errors quoted for the Dingle temperatures are rms errors of the least-squares fits.

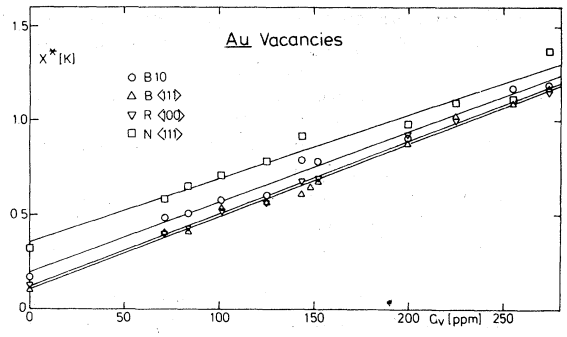

FIG. 3. Dingle temperatures X^* for four extremal cross sections in Au as a function of the vacancy concentration c_v. Intercept at $c_v = 0$ is attributed to the scattering of the conduction electrons at dislocations produced during the quenching process.

tions generated by the quench in our samples is not known. A rough estimate can be obtained in the following way. Chang and Higgins[6] observed in Cu Dingle temperatures of 0.43 K for the neck and 0.08 K for the belly ⟨111⟩ orbit per 10^7 dislocations/cm^2. If this value is used for Au as well, the intercept at $c_v = 0$ in Fig. 3 would be due to 8 $\times 10^6$ dislocations/cm^2 created during the quench. Figure 3 clearly demonstrates that it is necessary to measure the Dingle temperatures as a function of the vacancy concentration c_v for separating the contribution of the vacancies and of the dislocations in X^*. Table I gives a list of the Dingle temperatures per at.% vacancies in Au for the ten orbits investigated. The data analyzed include our preliminary results which were published in an earlier paper.[14] The cyclotron masses m_c^*/m_0 used in the analysis are included in the table.[9]

IV. DISCUSSION

A. Scattering anisotropy

The measured Dingle temperatures X^* are related to the local values of the scattering rates $1/\tau^*(\vec{k})$ by[4]

$$X^* m_c^* = \frac{\hbar^2}{(2\pi)^2 k_B} \oint \frac{k_\perp^2}{\vec{v}^* \circ \vec{k}_\perp} \frac{1}{\tau^*(\vec{k})}\, d\alpha \,. \tag{3}$$

α specifies the position of a representative point $\vec{k}_\perp$ on the cyclotron orbit. The weight factor $k_\perp^2/(\vec{v}^* \cdot \vec{k}_\perp)$ depends on the geometry of the Fermi surface and on the Fermi velocities $\vec{v}^*$. For the former we have used the five-coefficient symmetrized Fourier series representation for Au by Halse,[15] for the latter we have used our own data 5+ representation deduced from cyclotron-mass measurements.[9] Another Fourier-series representation with five coefficients was chosen for $1/\tau^*(\vec{k})$,

$$\frac{1}{\tau^*(\vec{k})} = T_{000} + T_{110} \sum \cos\frac{a}{2}k_x \cos\frac{a}{2}k_y + T_{200} \sum \cos a k_x + T_{211} \sum \cos a k_x \cos\frac{a}{2}k_y \cos\frac{a}{2}k_z + T_{220} \sum \cos a k_x \cos a k_y \,. \tag{4}$$

The sums are over cyclic permutations of x, y, and z. a is the lattice parameter of Au ($a = 4.0652$ Å). By means of the nonlinear least-squares fitting program VA05AD from the Harwell Subroutine Library the coefficients T_{lmn} were fitted to the ten Dingle temperatures in Table I according to Eq. (3). A five-coefficient representation was chosen in Eq. (4) for $1/\tau^*$ because it gave the best fit with the smallest number of coefficients. The values of the coefficients obtained are given in Table II. The fitted Dingle temperatures are compared to the measured data in Table I. Figure 4 is a plot of the scattering rates $1/\tau^*(\vec{k})$ along some high-symmetry directions on the Fermi surface. The graph

TABLE I. Dingle temperatures X^* per at.% vacancies in Au measured for ten extremal cross sections in the plane {110}. B, R, N, and D stand for belly, four-cornered rosette, neck, and dogsbone. Numbers without brackets give the angle in degrees by which the magnetic field is tilted against the crystallographic direction [001]. Cyclotron masses used in the analysis are taken from Ref. 9. Dingle temperatures quoted under T_{lmn} are calculated from the five coefficients Fourier-series fit described in the text [Eq. (4)].

	m_c^*/m_0	X^* (K/at.%) Experiment	T_{lmn}
$B\langle 100\rangle$	1.140	38.3 ± 2.5	38.5
B 10	1.084	37.2 ± 1.5	37.8
B 23	1.052	38.0 ± 1.3	37.3
$B\langle 111\rangle$	1.066	38.7 ± 1.1	38.9
B 60	1.071	37.7 ± 2.0	38.7
$R\langle 100\rangle$	1.014	38.6 ± 1.0	37.4
$N\langle 111\rangle$	0.280	33.8 ± 2.4	34.2
N 60	0.286	34.0 ± 2.0	34.2
D 85	1.003	38.9 ± 2.5	37.5
$D\langle 110\rangle$	0.983	37.0 ± 2.2	37.6

confirms what could be seen from the Dingle temperatures in Table I. There is only very little anisotropy in $1/\tau^*$ over the Fermi surface. We will come back to this point later.

B. Phase-shift analysis

In a recent series of papers,[16-18] Coleridge, Holzwarth, and Lee have elaborated on a generalized phase-shift analysis for the scattering of Bloch waves at defects in the noble metals. The scattering is parametrized in terms of Friedel phase shifts ϕ_L which depend on the scattering potential of the defect and on backscattering by the host lattice. $L=l,\Gamma$ labels the angular momenta l and the irreducible representations Γ on the cubic group to the different l (for a defect with cubic environment). In a nonrelativistic analysis it is

$$\tan\phi_L = \mathrm{Im}\chi_L/(\xi_l - \mathrm{Re}\chi_L) , \tag{5}$$

where ξ_l is defined by

$$\xi_l = (\cot\eta_l^h - \cot\eta_l^i)^{-1} , \tag{6}$$

η_l^h and η_l^i being the phase shifts for the host and the defect atoms, respectively, in muffin-tin approximation. The Brillouin-zone intergrals χ_L describe how the scattered wave emerging from the defect is backscattered by the host lattice thereby modifying the amplitude of the Bloch wave in magnitude and phase inside the defect muffin-tin sphere. The χ_L and η_l^h have been calculated for Au by Holzwarth and Lee.[17]

The Dingle temperatures are expressed in terms

TABLE II. Values of the coefficients T_{lmn} for the five coefficients Fourier-series fit [Eq. (4)]. Quality factor Q of the fit is smaller than the uncertainty of the experimental data (Table I).

	T_{lmn} (10^{13} sec^{-1}at.%$^{-1}$)
000	17.841717
110	41.220267
200	7.099074
211	5.017729
220	3.055403

$$Q = \left(\frac{1}{5}\sum_i (X_i^m - X_i^f)^2\right)^{1/2} = 1.1 \text{ K/at.\%}$$

of the ϕ_L and ξ_l as[17]

$$\frac{X^* m_c^*}{m_0} = c_v \frac{\epsilon_0}{k_B}\left(\frac{a_0}{a}\right)^2 \sum_L \frac{W_L}{\mathrm{Im}\chi_L} \sin^2\phi_L . \tag{7}$$

a_0 is the Bohr radius and $\epsilon_0 = e^2/2a_0$. c_v is the atomic fraction of vacancies. The W_L are orbital averages of the scattering anisotropy of the Lth lattice harmonics wave. The weight with which the different L contribute to the total anisotropy (as measured in the Dingle temperatures) depends on the host lattice and on the scattering strength of the defect through the factor $\sin^2\phi_L/\mathrm{Im}\chi_L$. The host orbital parameters W_L have been tabulated in Ref. 17 for the six stationary orbits ($\partial F/\partial\theta = 0$) in the plane {110}.

Using our Dingle temperatures for these six orbits we have fitted the η_l^i according to Eqs. (5)–(7) by means of a nonlinear least-squares fitting program (VA05AD Harwell Subroutine Library). Since the ϕ_L and η_l^i enter quadratically into the

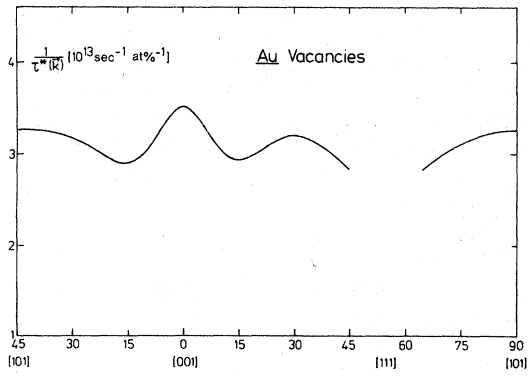

FIG. 4. Local values of the scattering rates $1/\tau^*(\vec{k})$ along some high-symmetry directions on the Fermi surface for the Au-vanancy system. Data are calculated from Eq. (4) and the coefficients of Table II. Anisotropy is only very weak.

TABLE III. Result of the phase shifts fit according to Holzwarth and Lee. Vacancy phase shifts η_l^i are fitted to six Dingle temperatures using Eqs. (5)–(7) in the text. Gold host lattice is treated nonrelativistically and relativistically. Although the fit is good, it is questionable if it is very significant because the phase-shift analysis does not take into account the strong lattice relaxation around the vacancy. It is significant that the Friedel sum F is not able to decide which one of the different combinations of the η_l^i (which are all compatible with the Dingle temperatures fit) is the correct one. (BTP denotes the turning point belly in the plane $\{110\}$.)

	Nonrelativistic				Relativistic			
	η_0^i	η_1^i	η_2^i	F	η_0^i	η_1^i	η_2^i	F
(1)	−0.4830	−0.3453	−0.3813	−1.284	−0.5093	−0.3478	−0.3759	−1.265
(2)	+0.5892	−0.3453	−0.3813	−0.859	+0.6072	−0.3478	−0.3759	−0.821
(3)	−0.4829	+0.5489	−0.3813	−0.345	−0.5317	+0.5448	−0.3715	−0.316
(4)	−0.4748	−0.3459	−0.0278	−0.078	−0.3542	−0.3440	−0.0219	−0.013
(5)	+0.5892	+0.5489	−0.3813	+0.080	+0.6122	+0.5448	−0.3715	+0.138
(6)	+0.5872	−0.3459	−0.0278	+0.343	+0.5695	−0.3440	−0.0219	+0.362
(7)	−0.4748	+0.5497	−0.0278	+0.861	−0.3872	+0.5397	−0.0325	+0.877
(8)	+0.5872	+0.5497	−0.0278	+1.282	+0.5780	+0.5397	−0.0325	+1.267

X^* (K/at.%)	Experiment	Fit Nonrelativistic	Fit Relativistic
$B\langle 100\rangle$	38.3 ± 2.5	38.3	38.3
BTP	38.0 ± 1.3	38.0	38.0
$B\langle 111\rangle$	38.7 ± 1.1	38.9	38.9
$R\langle 100\rangle$	38.6 ± 1.0	38.4	38.4
$N\langle 111\rangle$	33.8 ± 2.4	34.2	34.3
$D\langle 110\rangle$	37.0 ± 2.2	37.0	37.1

Dingle temperatures [Eq. (7)], the fit of the phase shifts is not unique. The possible combinations are given in Table III. In many cases it is possible to decide from the Friedel sum F which one is the correct combination of phase shifts. This does not work here, as will be shown later. Indeed, the application of the phase-shift analysis [Eqs. (5)–(7)] to the vacancy data presented here is rather problematic because this theory does not take into account the relaxation around the scattering center. But this is especially large for vacancies in Au.

Hertz *et al.*[19] found, from lattice-parameter changes, a volume change $\Delta V/V$ by vacancies of $\Delta V/V = -2.93\times 10^3 \rho_v/\Omega$ cm. Using $\rho_v = 1.69$ $\mu\Omega$ cm/at.%,[8] and $\gamma = 1.255$, the local volume change for a vacancy in Au is

$$(\Delta V/V)_{\text{loc}} = (1/\gamma)(\Delta V/V) = -0.40 \ . \tag{8}$$

This means that the effective volume of a vacancy in Au is not 1 but 0.6 atomic volume. The Friedel sum

$$F \equiv \sum_L \frac{2g_L\phi_L}{\pi} \tag{9a}$$

must be equal to

$$\Delta Z = -1 - (\Delta V/V)_{\text{loc}} = -0.60 \ . \tag{9b}$$

g_L is the degeneracy of the representation l, Γ. It is obvious from $\Delta Z = -0.60$ and from the values in Table III that the Friedel sum is inadequate to decide which one of the combinations for η_l^i is the correct one. A relativistic treatment of the gold host in the phase-shift analysis does not remove the ambiguity as is shown in Table III. The following model calculations of Dingle temperatures for vacancies in Au and Cu may help to clarify the influence of the lattice distortion on the scattering rates.

C. Model potential for vacancies in Au and Cu

We assume a gold lattice of touching muffin-tin spheres. The radius of the muffin-tin spheres is

$$r_{\text{MT}} = a\sqrt{2}/4 = 2.7160 a_0 \ . \tag{10}$$

If an Au atom is removed from the lattice and the relaxation around the vacancy is neglected, then the potentials of the neighboring atoms superpose to give a repulsive and rather flat potential in the vacancy. We therefore assume a constant potential V_0 above the muffin-tin zero V_{MT} as a potential for the vacancy in the defect muffin-tin sphere. The model is illustrated in Fig. 5 where the potential for an electron is sketched along an atom row

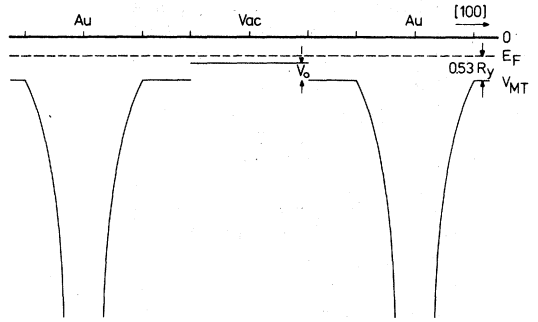

FIG. 5. Schematic drawing of the potential energy of an electron along a direction ⟨100⟩ in the Au lattice, illustrating the model of a vacancy used in the text. Lattice relaxation around the vacancy is not taken into account. V_0 is the potential energy in the vacancy above the muffin-tin zero V_{MT}. The Au muffin-tin radius r_{MT} is $2.7160a_0$.

⟨100⟩. The real potential will surely fall off somewhat at the border of the muffin-tin sphere. But we believe that this is a minor correction compared to the neglection of any relaxation around the vacancy. The model may therefore help to show what the influence of the relaxation on the Dingle temperatures is. The phase shifts η_l^i can be calculated analytically for this potential. Using the standard expression of the phase shifts in terms of the potential and the radial wave function[20] the model gives

$$\tan\eta_l^i = \frac{y j_l(x) j_{l-1}(y) - x j_{l-1}(x) j_l(y)}{y n_l(x) j_{l-1}(y) - x n_{l-1}(x) j_l(y)}, \qquad (11)$$

with

$$y = [(2m_0/\hbar^2)(E_F - V_0)]^{1/2} r_{MT},$$
$$x = [(2m_0/\hbar^2) E_F]^{1/2} r_{MT}.$$

j_l and n_l are spherical Bessel functions of the first and second kind.[21] Figure 6 is a plot of η_l^i as a function of V_0 for Au ($E_F = 0.53$ Ry). The phase shifts are predominantly s like, the p-phase shift being a factor of about 3.5 and the d-phase shift a factor of about 25 smaller than the s-phase shift. Using these phase shifts and the relativistic host parameters by Holzwarth and Lee,[17] Dingle temperatures were calculated for six orbits in gold. The result is shown in Fig. 7. The Dingle temperatures X^* per at.% vacancies are plotted vs V_0. The calculated data are renormalized for electron-phonon interaction. A nonrelativistic band structure for the Au lattice does not affect the data appreciably. The following features of Fig. 7 should

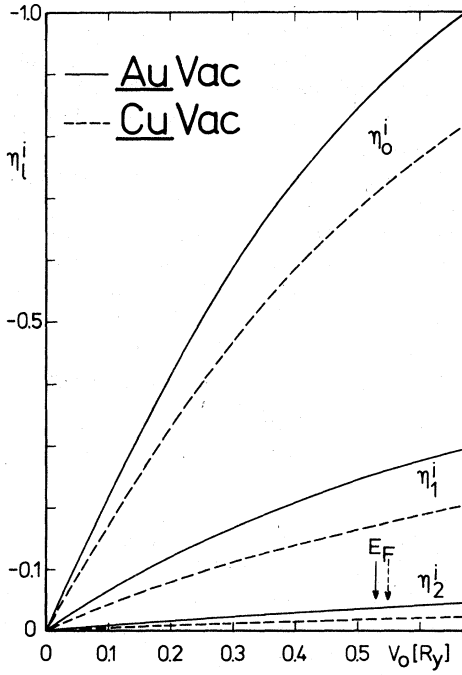

FIG. 6. Phase shifts η_l^i for vacancies in Au and Cu according to the model illustrated in Fig. 5 as a function of the repulsive potential V_0. Phase shifts are predominantly s-like.

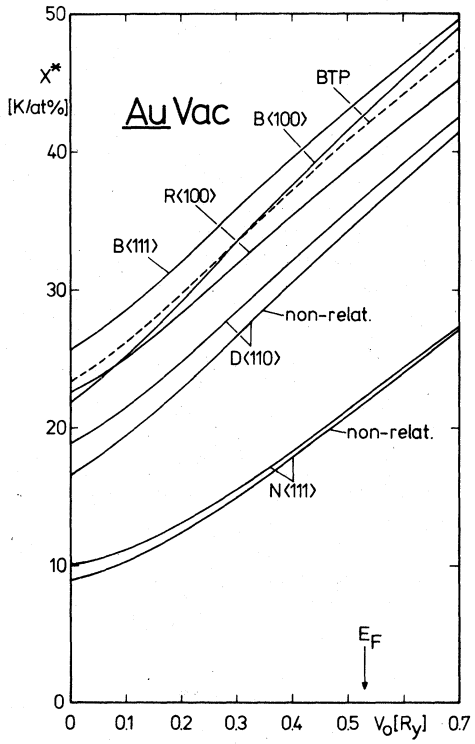

FIG. 7. Dingle temperatures for vacancies in Au calculated for the model shown in Fig. 5. Au lattice is treated relativistically. The Dingle temperatures for the belly orbits are about a factor 2 larger than the neck Dingle temperatures. Nonrelativistic treatment of the Au lattice does not affect the data appreciably.

be emphasized. The Dingle temperatures for the belly and rosette orbits are nearly equal to one another in agreement with the experimental results. But they are about a factor of 2 larger than the neck Dingle temperatures in contrast to the experimental results. This behavior is nearly independent of the values of V_0. If the vacancy potential used in this calculation is realistic, the discrepancy between theory and experiment has to be attributed to the lattice distortion around the vacancy. Furthermore, for a reasonable range of the values of V_0 ($V_0 \lesssim E_F$), the neck data are more affected by the lattice relaxation than the belly data are. Assuming even that only the necks are affected by the relaxation, a value $V_0 = 0.40$ Ry would bring the three belly Dingle temperatures in good agreement with the experimental results. The neck value would be too small by a factor of 1.8. The dogsbone and rosette data would be only somewhat smaller than the experimental results in accordance with the fact that these orbits cover both belly and neck parts of the Fermi surface.

The Friedel sum [Eq. (9a)] was calculated for the model. It is shown in Fig. 8. At $V_0 = 0.40$ Ry, $F = 0.055$. The only combination of negative phase shifts in Table III with a small value for η_2^i, as predicted by Fig. 6, is the combination (4). It gives a Friedel sum of -0.078 in crude agreement with the value 0.055. But it should be noted that both values for F are in complete disagreement with $\Delta Z = -0.60$ [Eq. (9b)]. Our vacancy model, although crude, gives therefore strong evidence that the lattice distortion around a vacancy has to be taken into account in any description of the scattering rates. An empty lattice place creates relatively little neck scattering. The relaxation around it enhances preferentially the neck scattering, so that the scattering rates measured in the Dingle temperatures are rather isotropic. Phase shifts, Dingle temperatures, and Friedel sums have been calculated for the same type of vacancy model in copper with $r_{MT} = 2.4072 a_0$ and $E_F = 0.55$ Ry. The corresponding data are shown in Figs. 6, 9, and 8. Although the phase shifts η_l^i are rather similar, the Dingle temperatures show much less anisotropy than in the case of gold. No reliable experimental Dingle temperatures are available at present time to be compared with the calculations.

V. CONCLUSIONS

Dingle temperatures for vacancies in Au have been presented in this paper. It has been shown how the influence of vacancies and dislocations produced during the quenching process can be separated. The scattering rates vary only weakly over the Fermi surface of gold. The crucial point

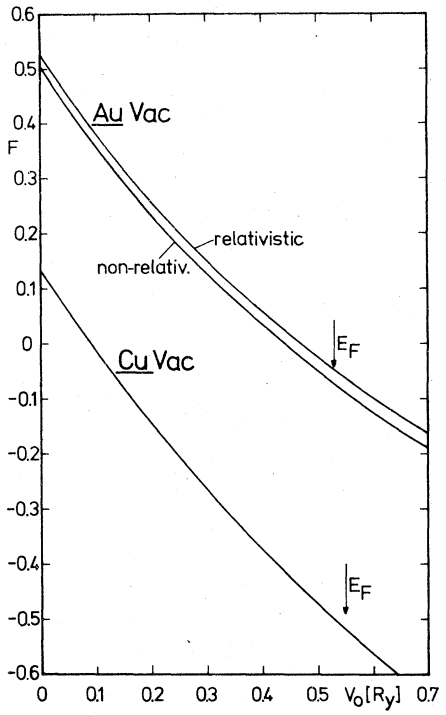

FIG. 8. Friedel sum calculated for the vacancy model illustrated in Fig. 5 for Au and Cu.

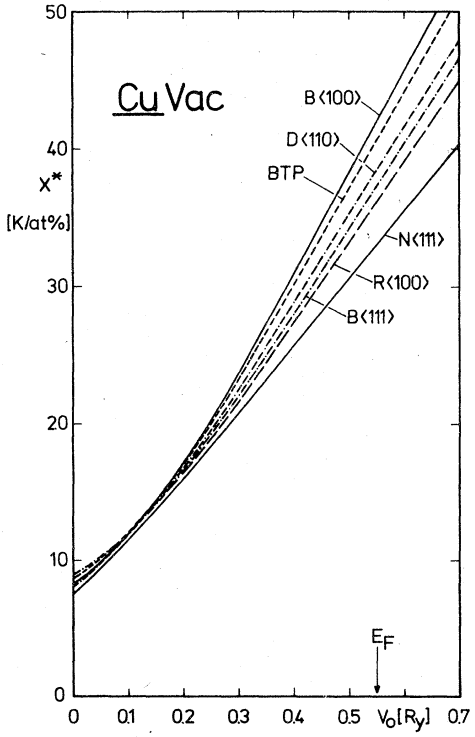

FIG. 9. Dingle temperatures for vacancies in Cu calculated for the model shown in Fig. 5.

in the analysis of the data is the influence of lattice distortion around the vacancy on the scattering rates. The lattice relaxation will not only alter the phase shifts η_l^i of the defect, but also the backscattering and the anisotropy of the T matrix. A general theory for the electron-impurity scattering with lattice distortion has been given recently by Lodder.[22] Unfortunately, the theory has not yet been elaborated to such a degree that the data presented here could be analyzed in terms of it. Another approach to the influence of lattice distortion around a vacancy on the scattering rates is the measurement of Fermi surface changes due to the vacancies. It is believed that the phase shifts derived from defect-induced Fermi-surface changes are more accurate because they include a correction for the uniform expansion of the lattice and because the anisotropy of the Fermi surface is relatively unaffected by the localized distortion.[18,23] Further experimental investigation on vacancies in gold can help to clarify this point.

ACKNOWLEDGMENTS

The author would like to thank Dr. N. A. W. Holzwarth, Dr. P. H. Dederichs, and Dr. R. O. Jones for many helpful discussions and Dr. E. Seitz for carefully reading the manuscript.

[1]R. G. Poulsen, D. L. Randles, and M. Springford, J. Phys. F 4, 981 (1974).
[2]H. R. Brown and A. Myers, J. Phys. F 2, 683 (1972).
[3]D. Sang and A. Myers, J. Phys. F 6, 545 (1976).
[4]D. H. Lowndes, K. M. Miller, R. G. Poulsen, and M. Springford, Proc. R. Soc. A 331, 497 (1973).
[5]W. R. Wampler and B. Lengeler (unpublished).
[6]Y. K. Chang and R. J. Higgins, Phys. Rev. B 12, 4261 (1975).
[7]Y. K. Chang, A. J. Arko, G. W. Crabtree, J. B. Ketterson, L. R. Windmiller, R. J. Higgins, and F. W. Young, in Fundamental Aspects of Radiation Damage in Metals, Proceedings of the International Conference, Gatlinburg, Tennessee, 1975 (unpublished), p. 846.
[8]B. Lengeler, Philos. Mag. 34, 259 (1976).
[9]B. Lengeler, W. R. Wampler, R. R. Bourassa, K. Mika, K. Wingerath, and W. Ueloff (unpublished).
[10]M. Abdel-Fattah, V. Sorajic, and W. Uelhoff, Berichte der KFA Jülich, JÜL-944-FF (1973) (unpublished).
[11]S. Mantl and W. Triftshäuser, Phys. Rev. Lett. 34, 1554 (1975).
[12]R. W. Siegel, Philos. Mag. 13, 337 (1966).
[13]J. J. Jackson, Proceedings International Conference on Lattice Defects in Quenched Metals, Argonne 15–17 June 1964, edited by R. M. J. Cotterill, M. Doyama, J. J. Jackson, and M. Meshii (unpublished), p. 479.
[14]B. Lengeler and W. Uelhoff, Phys. Lett. A 53, 139 (1975).
[15]M. R. Halse, Philos. Transact. R. Soc. Lond. 265, 507 (1969).
[16]P. T. Coleridge, N. A. W. Holzwarth, and M. J. G. Lee, Phys. Rev. B 10, 1213 (1974).
[17]N. A. W. Holzwarth and M. J. G. Lee, Phys. Rev. B 13, 2331 (1976).
[18]M. J. G. Lee, N. A. W. Holzwarth, and P. T. Coleridge, Phys. Rev. B 13, 3249 (1976).
[19]W. Hertz, W. Waidelich, and H. Peisl, Phys. Lett. A 43, 289 (1973).
[20]E. Merzbacher, *Quantum Mechanics* (Wiley, New York, 1961), p. 241.
[21]M. Abramowitz and I. A. Stegun, *Handbook of Mathematical Functions*, (Dover, New York, 1965).
[22]A. Lodder, J. Phys. F 6, 1885 (1976).
[23]P. T. Coleridge, J. Phys. F 5, 1317 (1975).